Research Square

Preprints are preliminary reports that have not undergone peer review.
They should not be considered conclusive, used to inform clinical practice,
or referenced by the media as validated information.

Cellulose–protein supramolecular entangled networks enable bioplastics with ultrahigh strength and broad-temperature stability

Dawei Zhao

daweizhao@syuct.edu.cn

Shenyang University of Chemical Technology; Northeast Forestry University https://orcid.org/0000-0003-2813-7263

Jiying Chu

Shenyang University of Chemical Technology

Minxin Wang

Shenyang University of Chemical Technology

Changhong Lin

Shenyang University of Chemical Technology

Geyuan Jiang

Northeast Forestry University

Suqing Zeng

NEFU

Guanglei Chen

Shengjing Hospital of China Medical University

Haipeng Yu

Northeast Forestry University https://orcid.org/0000-0003-0634-7913

Article

Keywords: cellulose, supramolecular network, bioplastic, mechanical performance, structural stability

Posted Date: September 15th, 2026

DOI: https://doi.org/10.21203/rs.3.rs-10707870/v1

License: This work is licensed under a Creative Commons Attribution 4.0 International License.
Read Full License

Additional Declarations: There is **NO** Competing Interest.

Abstract

Developing bioplastics that combine high mechanical robustness, structural stability across a broad temperature range, and non-petrochemical origins remains challenging. Herein, we report an entirely biomass-derived supramolecular bioplastic (BS–bioplastic) fabricated from cellulose and soy protein isolate via network reconstruction. Enabled by dense hydrogen-bonding interactions and an entangled supramolecular architecture, BS–bioplastic exhibits a tensile strength of 125.85 ± 3.16 MPa and a flexural modulus of 8.30 ± 0.22 GPa, while remaining structurally stable from − 196 to 180°C. After exposure to − 196°C for 30 min or 180°C for 2 h, it retains its intact morphology and a tensile strength exceeding 85 MPa—performance that, to the best of our knowledge, has not been achieved by either bio-based or petrochemical plastics. BS–bioplastic further allows ethanol-assisted programmable three-dimensional shaping and undergoes complete biodegradation under natural conditions. Economic analysis suggests its potential for scalable production, recycling, and reuse. This work demonstrates a feasible route to high-performance bioplastics derived entirely from biomass and establishes BS–bioplastic as a sustainable structural material for future applications.

Introduction

Plastics have evolved from conventional petrochemical plastics to wood–plastic composites and, more recently, to bioplastics. Petrochemical plastics are manufactured by chemical synthesis from fossil-based feedstocks[1], such as petroleum and natural gas. Their widespread use stems from their favorable mechanical properties, ease of processing and low cost. However, their persistence in the environment, low recycling rates and associated pollution (left panel of Fig. 1a) have raised growing concern[2–4]. In particular, the extensive accumulation of nondegradable plastic waste in terrestrial and marine environments causes severe and often irreversible damage to ecosystems[5–8].

To improve the environmental sustainability of plastics, renewable and eco-friendly resources—including wood, bamboo, and corn straw—are introduced as reinforcing components in plastic composites[9–12]. Wood–plastic composites (middle panel of Fig. 1a) are typically produced by incorporating biomass particles or cellulose fibers into petrochemical matrices such as polyvinyl chloride (PVC), acrylonitrile–butadiene–styrene (ABS), and polyethylene (PE)[13–16]. Although this strategy reduces reliance on fossil-based feedstocks, several challenges remain unresolved, including plastic-waste accumulation, poor degradability, thermal expansion and brittle fracture[17–20].

In contrast to cellulose-fiber reinforcement, the molecular-level design[21–23] and utilization of cellulose[24,25] for fabricating bioplastic have attracted increasing attention (right panel of Fig. 1a). By constructing hydrogen-bonding (H-bonding) networks among cellulose molecules and regulating their molecular assembly[21,26–28], researchers have developed bioplastics with natural degradability and recyclability[29–31]. In addition, the construction of solvent-responsive supramolecular network using cellulose as a molecular scaffold endows the bioplastics with improving mechanical properties and

moldability[32,33]. However, the additional polymers incorporated into these supramolecular networks are generally derived from petrochemical sources[32–35], as exemplified by polyacrylamide. As a result, these bioplastics continue to face challenges, including difficulty in achieving tensile strength exceeding 110 MPa and insufficient stability under both ultralow temperatures (for example, − 196°C) and elevated temperatures (for example, above 150°C).

Herein, we developed an entirely biomass-derived BS–bioplastic through ethanol-induced reconstruction of a cellulose–soy protein isolate (SPI) supramolecular network. As a biopolymer formed by dehydration-condensation of amino acids, SPI contains amide structure (–NH–C = O–) in its molecular backbone and carboxyl groups (–COOH) in its side chains, which enable H-bonds with cellulose and facilitate the formation of an entangled supramolecular architecture during ethanol treatment. As shown in Fig. 1b, the resulting BS-bioplastic can be readily scaled to dimensions exceeding 100 cm and exhibits robust mechanical performance, including a tensile strength above 120 MPa and a flexural modulus exceeding 8 GPa, as well as structural stability over an ultrawide temperature range from − 196 to 180°C. Even after exposure to − 196°C for 30 min or 180°C for 2 h, its tensile strength and elastic modulus remain above 85 MPa and 1 GPa, respectively (Fig. 1c).

Compared with commercial plastics, including ABS, polymethyl methacrylate (PMMA), and polylactic acid (PLA), BS–bioplastic offers a compelling combination of thermal stability, mechanical performance, processability, and complete biodegradability (Fig. 1d). In addition, its entirely bio-based supramolecular network enables BS–bioplastic to be readily shaped into products with designable three-dimensional geometries, including honeycomb panels, storage boxes, food containers, and industrial gears (Fig. 1e), broadening its potential applications in buildings, smart packaging, and precision electronics.

Results

Design and molecular dynamics (MD) simulations of BS–bioplastic

Bamboo cellulose and SPI were used to construct an interpenetrating and entangled supramolecular network (Supplementary Fig. 1). First, SPI molecules were incorporated into the cellulose molecular network to form cellulose-SPI supramolecular system. Ethanol was then used to induce structural reorganization, resulting in the formation of an entangled supramolecular architecture within BS–bioplastic (Fig. 2a). During this process, the –NH–C = O– and –COOH groups on the SPI molecule can form periodically arranged H–bonds with the hydroxyl (–OH) groups of cellulose molecules, which enables the fixed-point adsorption of SPI molecules onto cellulose molecular chains. Ethanol treatment would guide the SPI molecules to curl and entangle along the cellulose molecular skeleton, thereby generating a dense, physically entangled supramolecular network in BS–bioplastic. This unique structure will restrict the migration of supramolecular segments, suppress brittle fracture, and enhance the structural stability of BS–bioplastic at both cryogenic and elevated temperatures.

MD simulations (Fig. 2b-e) further elucidated the evolution and formation of entangled supramolecular architecture in BS–bioplastic. Root-mean-square deviation (RMSD) analysis shows that cellulose molecules remain stable in the cellulose-SPI supramolecular gel (noted as C–SPI gel), and only undergo minimal changes in BS–bioplastic, indicating that both systems have reached dynamic equilibrium (Fig. 2b). Although the SPI molecules exhibited minimal conformational changes in C–SPI gel, their RMSD increased rapidly in BS–bioplastic (Fig. 2b), suggesting that the SPI chains underwent structural reconfiguration following ethanol treatment.

The end-to-end distance of cellulose differed only slightly between C–SPI gel and BS–bioplastic. In contrast, the SPI molecules exhibited a consistently shorter end-to-end distance in BS–bioplastic, indicating that they adopted a more compact, curled conformation within BS–bioplastic (Fig. 2c). Compared with C–SPI gel, BS–bioplastic contained a greater number of H-bonds between cellulose–cellulose, cellulose–SPI, and SPI–SPI pairs (Fig. 2d). As a result, the curled SPI molecules wrapped around the cellulose chains (Fig. 2a), forming a denser and entangled supramolecular architecture in BS–bioplastic. Consistent with this interpretation, MD snapshots revealed denser interactions between cellulose and SPI molecules in BS–bioplastic than in C–SPI gel (Fig. 2e). This architecture will facilitate stress redistribution, enhance mechanical strength, and endow BS–bioplastic with structural robustness under both high- and low-temperature conditions.

As shown in Fig. 2f, this molecular-scale reorganization increased the macroscopic structural rigidity of BS–bioplastic, enabling the fabrication of diverse geometries through injection molding, compression molding, and other processing methods. The resulting shaped BS–bioplastic exhibited high mechanical toughness, maintaining its structural integrity under substantial bending (Fig. 2g) and resisting damage under an applied load exceeding 500 times its own weight (Supplementary Fig. 2).

Structure and performances of BS–bioplastic

To further investigate the structural evolution of BS–bioplastic, we employed a range of analytical and characterization techniques. As shown in Fig. 3a, the flexible and soft C–SPI gel was transformed into a rigid yet tough BS–bioplastic following ethanol treatment. Super-depth-of-field microscopy revealed a substantial increase in surface roughness and height variation in BS–bioplastic (Supplementary Fig. 3). Scanning electron microscopy (SEM) further showed that BS–bioplastic exhibited a more homogeneous and compact morphology than that of C–SPI gel (Fig. 3b). Raman spectroscopy also revealed a substantial increase in signal intensity for BS–bioplastic (Supplementary Fig. 4). These observations suggest that ethanol promotes the formation of a dense and compact network structure in BS–bioplastic. Compared with C–SPI gel, the characteristic –OH absorption band in Fourier-transform infrared (FTIR) spectrum of BS–bioplastic was narrower, whereas the characteristic C–O peak was sharper (Fig. 3c). This indicates that BS–bioplastic exhibits enhanced and strong H-bonding interaction between cellulose and SPI molecules, which suppresses the vibrations and mobility of molecular chains. X-ray photoelectron spectroscopy (XPS) provided further support for this interpretation. As shown in Supplementary Fig. 5, all characteristic peaks within BS–bioplastic shifted toward lower binding

energies, suggesting changes in the chemical environments of the constituent functional groups. This is attributed to the strong H-bonding interaction between cellulose and SPI in BS–bioplastic, which increase the electron density around the atoms and consequently lead to a decrease in binding energy.

To elucidate the supramolecular architecture of BS–bioplastic, we conducted X-ray diffraction (XRD), small-angle X-ray scattering (SAXS), and wide-angle X-ray scattering (WAXS) analyses. In the XRD pattern, BS–bioplastic exhibits sharper crystalline diffraction peaks than that of C–SPI gel, indicating the formation of more compact supramolecular architecture of BS–bioplastic (Supplementary Fig. 6). As shown in Fig. 3d, two-dimensional (2D) FTIR spectrum shows the markedly increased integrated intensity of BS–bioplastic compared to that of C–SPI gel, demonstrating the presence of dense H-bonding network in BS–bioplastic.

In addition, the WAXS profiles, together with the 2D SAXS and WAXS images, show the stronger signal intensities and more pronounced scattering rings for BS–bioplastic (Fig. 3e, f and Supplementary Fig. 7). These results confirm that ethanol-induced structural reconfiguration promotes intermolecular entanglement of cellulose and SPI, generating an entangled supramolecular structure in BS–bioplastic. This combination of a densified H-bonding network and an entangled, compact supramolecular architecture is expected to confer attractive mechanical properties and broad high- and low-temperature resistance to BS–bioplastic.

Nanoindentation tests were used to characterize the microscale mechanical properties of BS–bioplastic. Under the same applied load, BS–bioplastic exhibited a lower indentation depth than the commercial plastics ABS and PVC (Fig. 3g), indicating greater resistance to indentation. Although its nanoindentation hardness was lower than those of commercial plastics (Fig. 3h), this dense and entangled supramolecular architecture in BS–bioplastic will facilitate the dissipation of localized stresses and suppress brittle fracture induced by stress concentration. As shown in Fig. 3i, BS–bioplastic exhibited a higher nanoindentation modulus than ABS, PMMA, PVC, and PLA. In addition, cyclic tensile tests (Supplementary Fig. 8) showed that BS–bioplastic can dissipate impact- and fatigue-induced energy through limited plastic deformation, providing effective protection and extending its service life.

Mechanical properties of BS–bioplastic

Compared with C–SPI gel, BS–bioplastic, composed of 93 wt% cellulose and 7 wt% SPI (Supplementary Fig. 9), exhibits a high tensile strength of over 120 MPa and an elastic modulus of over 1.4 GPa (Supplementary Fig. 10), both of which substantially exceed the corresponding values of 0.67 ± 0.02 MPa and 1.3 ± 0.19 MPa for C–SPI gel.

We next conducted a comprehensive comparison of the mechanical performance of BS–bioplastic with that of several commercial plastics, including ABS, PMMA, and PLA. As shown in Fig. 4a, BS–bioplastic exhibits a distinctive tensile stress–strain curve, with the stress increasing sharply with strain in the

elastic deformation regime. At a strain of 15%, BS–bioplastic reaches a yield plateau associated with plastic flow and can sustain a total elongation exceeding 30%, indicating good extensibility. Compared with ABS, PMMA, PVC, PLA, and several previously reported bioplastics[33,35,37–41], BS–bioplastic exhibits a higher tensile strength of 125.85 ± 3.16 MPa (Fig. 4b) and an elastic modulus of 1.44 ± 0.05 GPa (Fig. 4c). In addition, BS–bioplastic exhibits a toughness of 20.2 MJ m^{-3}, exceeding those of ABS, PMMA, PLA, and PVC (Supplementary Fig. 11).

Three-point bending tests further demonstrate the good flexural performance of BS–bioplastic. As shown in Fig. 4d, BS–bioplastic displays a distinct yielding behavior in its flexural stress–strain response, which can be attributed to its dense, entangled supramolecular architecture. This architecture facilitates stress redistribution and enhances the BS–bioplastic's toughness and energy-absorption capacity. Accordingly, BS–bioplastic exhibits a flexural strength of reaching 92.01 ± 2.77 MPa and a flexural modulus of up to 8.30 ± 0.22 GPa (Fig. 4e, f), both of which are substantially higher than those of common commercial plastics, including ABS, PMMA, PVC, and PLA.

Notably, BS–bioplastic exhibits promising impact and puncture resistance. Impact-resistance tests were performed using a drop-weight impact tester (Fig. 4g). Comparison of optical images before and after impact revealed that BS–bioplastic maintained its structural integrity after an 8 kg hammer was dropped from a height of 300 mm. In contrast, commonly used commercial plastics, including ABS, PLA, and polyethylene terephthalate (PET), sustained severe damage at impact heights below 300 mm (Fig. 4h). From the Fig. 4i, BS–bioplastic exhibited an impact energy of reaching 23.5 J, exceeding those of all the commercial plastics tested. To quantitatively evaluate the local load-bearing capacity of BS–bioplastic, puncture-resistance tests were conducted on BS–bioplastic and several commercial plastics. The puncture force–displacement curves show that BS–bioplastic offers substantially greater resistance to deformation than commercial plastics such as PMMA and PLA (Fig. 4j). Following puncture, the resulting hole in BS–bioplastic specimen remained centered (inset in Fig. 4j), indicating the reliability of puncture measurements. As shown in Fig. 4k, BS–bioplastic exhibited a puncture force of 112.93 ± 3.46 N and a puncture energy of 157.20 ± 9.53 mJ, both of which were higher than those of the commercial plastics. These outstanding impact- and puncture-resistance properties highlight the considerable potential of BS–bioplastic for applications in aerospace protective equipment.

Structural stability at low and high temperatures

We evaluated the stability of BS–bioplastic and several commercial plastics over a broad temperature range. Dynamic mechanical analysis (DMA) was performed to assess the thermal stability of BS–bioplastic and four commercial plastics: ABS, PMMA, PLA, and polypropylene (PP). As shown in Fig. 5a, BS–bioplastic exhibited a relatively high storage modulus over the temperature range of − 50 to 160°C. Even at 160°C, its storage modulus remained as high as 1,069.62 MPa. Compared with these commercial plastics (Fig. 5b, c), BS–bioplastic displayed smooth, approximately linear loss modulus–temperature and loss tangent (tan δ)–temperature profiles over the range of − 50 to 160°C. These

results, together with the images presented in Supplementary Fig. 12, demonstrate that BS–bioplastic can maintain its structural integrity and mechanical toughness at temperatures ranging from − 50 to 160°C.

We further evaluated the high-temperature resistance and low-temperature tolerance limits of BS–bioplastic. After exposure to 180°C for 2 h, BS–bioplastic still retained its structural integrity without thermal deformation (Fig. 5d). In contrast, PMMA, ABS, and PP underwent severe structural deformation under the same conditions. Moreover, even after prolonged exposure to this high temperature, BS–bioplastic retained good toughness, showing no visible damage after bending or folding—an outcome not observed for PLA, which fractured upon bending. Consistent with the SEM observations (Supplementary Fig. 13), BS–bioplastic retained a dense and cohesive microstructure after exposure to 180°C for 2 h. Comparison of the macroscopic mechanical properties of BS–bioplastic and commercial plastics at high temperature (Fig. 5e, f) further revealed that BS–bioplastic exhibited high mechanical performance, with a tensile strength of 111.42 MPa and an elastic modulus of 1.53 GPa. These high-temperature mechanical properties were significantly superior to those of most commercial plastics (Fig. 5g), including the engineering plastic polyamide 66 (PA66).

In addition, BS–bioplastic also exhibits good structural stability and mechanical performance at low temperatures. As shown in Fig. 5h, after exposure to liquid nitrogen (− 196°C) for 30 min, the BS–bioplastic retained its structural integrity and did not undergo brittle fracture, even when substantially folded. In contrast, commercial plastics, including ABS, PMMA, and PLA, experienced severe structural damage upon bending (Fig. 5h and Supplementary Fig. 14). Mechanical tensile tests were performed immediately after liquid-nitrogen treatment. As shown in Fig. 5i, BS–bioplastic maintained high deformation resistance at low strains, together with good toughness and extensibility at high strains. Its tensile strength and elastic modulus reached 86.88 MPa and 1.13 GPa, respectively (Fig. 5j), exceeding those of ABS, PMMA, and PLA. This mechanical strength and toughness of BS–bioplastic at extremely low temperatures may be attributed to the compact, entangled supramolecular architecture formed by cellulose and SPI, which provides BS–bioplastic with a certain degree of segmental mobility and strain-buffering capacity. The unique structural robustness and favorable mechanical properties of BS–bioplastic over a broad temperature range make it a promising candidate for applications in cryogenic engineering, aerospace, medical devices, and related fields.

Biodegradability, recyclability, and economic feasibility

Human neonatal dermal fibroblasts (NHDFs) were selected to evaluate the cytotoxicity of BS–bioplastic. As shown in Fig. 6a, the relative viability of NHDFs exceeded 100% after treatment with BS–bioplastic extracts at various concentrations, indicating that BS–bioplastic possesses good biofriendliness and may promote cell proliferation. Confocal live-cell imaging further confirmed its favorable biofriendliness, with only a small number of dead cells observed throughout the cultivation period (Fig. 6b). These results highlight the potential of BS–bioplastic for biosafety-sensitive applications, particularly in healthcare.

In addition to its biocompatibility, the biodegradability of BS–bioplastic provides a promising approach for mitigating the ecological risks associated with persistent plastic waste in soil ecosystems. During an outdoor soil-degradation experiment, BS–bioplastic underwent progressive morphological disintegration and was completely degraded within 90 days (Fig. 6c). After 60 days, SEM images revealed extensive microbial colonization on the surface of BS–bioplastic companied by partial disintegration of its internal structure (inset in Fig. 6d). The residual mass fraction gradually decreased to nearly zero during degradation, demonstrating the complete degradability of BS–bioplastic (Fig. 6d).

The recyclability of BS–bioplastic further provides a viable pathway toward material circularity and sustainable development. A closed-loop recycling process was established in which damaged fragments and recovered [Bmim]Cl were used to fabricate recycled BS–bioplastic (re–BS–bioplastic), thereby enabling multiple recycling cycles (Fig. 6e). Throughout the recycling process, re–BS–bioplastic retained its excellent processability and three-dimensional shapeability (Supplementary Fig. 15). Notably, even after five recycling cycles, re–BS–bioplastic maintained favorable mechanical properties, including a tensile strength exceeding 70 MPa (Fig. 6f) and an elastic modulus of 786.65 MPa (Supplementary Fig. 16).

Economic feasibility is another critical factor for the large-scale production. We conducted a techno-economic analysis (TEA) comparing BS–bioplastic with ABS, PP, PVC, PMMA, and PLA (Fig. 6g and Supplementary Tables 1 and 2). The estimated production cost of BS–bioplastic is approximately $3,174.75 per ton, higher than that of petrochemical plastics. Electricity accounted for only 2.49% of the total cost, suggesting that optimizing energy consumption would have limited potential for cost reduction compared with improving solvent recovery and reuse. By contrast, [Bmim]Cl accounted for 53.55% of the total cost; however, its recovery and reuse could substantially reduce the overall production cost. Ethanol represented 39.81% of the total cost and played a critical role in reconstructing the supramolecular architecture of BS–bioplastic. Therefore, enabling the recycling and reuse of ethanol in future work could further reduce manufacturing costs.

Collectively, although the current production cost of BS–bioplastic moderately exceeds that of conventional plastics, its distinctive combination of mechanical robustness, exceptional structural stability across a broad temperature range, inherent biodegradability, designable shapeability, and recyclability may well offset this cost premium. These attributes position BS–bioplastic as a competitive and sustainable alternative for high-performance applications where both environmental footprint and functional reliability are critical.

Discussion

In summary, we propose a feasible strategy for producing high-performance bioplastics from renewable cellulose and SPI through supramolecular network transformation. The resulting BS–bioplastic exhibits high mechanical strength and reliable structural stability across a broad temperature range (− 196 to 180°C), addressing a longstanding challenge in the development of bioplastics. Compared with

commercial plastics, BS–bioplastic exhibits a high mechanical tensile strength of over 120 MPa, an elastic modulus of 1.4 GPa, and a flexural modulus of over 8 GPa. It also demonstrates attractive impact and puncture resistance. These properties are attributed to the dynamic cross-linking of H-bonds and the formation of a dense, entangled supramolecular architecture within BS–bioplastic. After exposure to either − 196°C for 30 min or 180°C for 2 h, the mechanical tensile strength and elastic modulus of BS–bioplastic remain above 85 MPa and 1 GPa, respectively. This broad temperature tolerance helps prevent softening at elevated temperatures and brittle fracture under cryogenic conditions, expanding the potential applications of BS–bioplastic in aerospace and automotive interiors.

In addition, BS–bioplastic exhibits promising processability and dimensional scalability for large-scale manufacturing. It can be fabricated into a variety of geometries, making it suitable for potential applications such as smart building components, protective structures, and mechanical parts exposed to temperature fluctuations. From an environmental perspective, BS–bioplastic can undergo complete biodegradation in soil within 90 days. It can also be recycled and reused while retaining its outstanding mechanical properties and resistance to high and low temperatures. TEA indicates that large-scale production is feasible, suggesting that BS–bioplastic could reduce reliance on petrochemical plastics and contribute to the sustainable development of the bioplastics industry.

Nevertheless, several challenges must be addressed before BS–bioplastic can be commercialized and adopted in everyday applications. These challenges include improving solvent-recovery efficiency, developing greener molding processes, and evaluating the service life of products intended for use in construction, automotive components, packaging, and other applications.

Methods

Material

Bamboo stems, 1-butyl-3-methylimidazolium chloride ([Bmim]Cl), anhydrous ethanol, and SPI were purchased from Aladdin (Shanghai, China).

Preparation of bamboo cellulose

Bamboo chips were delignified in a 10 vol% peroxyformic acid solution at 50°C for 12 h. The treated chips were then neutralized with a 0.5 wt% sodium hydroxide solution for 5–10 min and washed several times with deionized water to remove residual chemicals and detach the parenchymal cells from the cellulose macrofibers. The samples were subsequently dried at room temperature. The peroxyformic acid solution, which contained 1 wt% sulfuric acid, was prepared by mixing 30% hydrogen peroxide with formic acid at a molar ratio of 1:1.

Preparation of C–SPI gel

The 35 g [Bmim]Cl and 6.18 g of dried bamboo cellulose were mixed in a 250 ml three-mouth flask which was washed and dried, and mechanically stirred in an oil bath at 85°C for 4 h to obtain a cellulose

supramolecular system. When the temperature of the oil bath pot was adjusted to 65°C, 0.41 g of SPI was added and then we continue stirred for 4 h to obtain the cellulose-SPI supramolecular system. We applied the gel evenly on the clean glass plate and placed it in a circulating drying oven at 65°C for at least 12 h. After all the bubbles were eliminated, we soaked it in water for 5 h (changed the water 1–2 times in the middle) to obtain C–SPI gel.

Construction of BS–bioplastic

The C–SPI gel was soaked in ethanol solution for stimulation treatment over a period of 12 h. Then, in order to completely evaporate the ethanol, we took it out and placed it in open air for 7 days to obtain BS–bioplastic.

Dimensional stability tests. In an elevated-temperature environment, some commercial plastics and BS-bioplastic with dimensions of 40 × 40 × 1 mm were placed in a constant temperature test chamber (180°C) to test their dimensional stability. After being exposed to 180°C for 2 hours, the samples were taken out and cooled them at room temperature for 10 min, then their macroscopic deformation (such as warping and melting) was observed and their dimensions were measured. Each sample was measured five times.

Biodegradability tests. To assess the biodegradability of various materials including ABS, PMMA, PP, PET, PLA and BS-bioplastic, samples were prepared and subsequently buried at a depth of 10 cm in natural soil. Periodically, these specimens were retrieved for evaluation, and their morphological changes were recorded using digital photography.

Recycling of [Bmim]Cl. The aqueous washing solution obtained from multiple water-exchange steps of C–SPI gel was collected. The solution was filtered to remove impurities, and water was then removed by rotary evaporation under vacuum to recover the [Bmim]Cl.

Data Availability Statement

The data that support the findings of this study are available from the corresponding author upon reasonable request.

Declarations

Acknowledgements

D.Z. acknowledges the support by the National Natural Science Foundation of China (Grant No. 32371823), the Liaoning Province Xingliao Talents Leading Talent Program (Grant No. XLYC2402043), and the Key Project in Science & Technology of SYUCT (Grant No. 2024DB001). H.Y. acknowledges the support by the National Natural Science Foundation of China (Grant No. 32330072).

Author contributions

D.Z. and H.Y. supervised the project and designed the experiments. J.C. carried out most of the experiments. C.L. and M.W. participated in the experiments and contributed to the analysis of mechanical performances and microstructure. G.J. and S.Z. provided valuable contributions to the analysis of thermal performance and the assessment of cytotoxicity. J.C. wrote the paper. D.Z., G.C. and H.Y. discussed the results, designed the mechanism and collectively reviewed the paper. All authors discussed the results and commented on the manuscript.

Competing interests

The authors declare that they have no competing interests.

References

1. Geyer, R., Jambeck, J. R. & Law, K. L. Production, use, and fate of all plastics ever made. *Sci. Adv.* **3**, e1700782 (2017).
2. Bergeson, A. R., Silvera, A. J. & Alper, H. S. Bottlenecks in biobased approaches to plastic degradation. *Nat. commun.* **15**, 4715 (2024).
3. OECD. *Global Plastics Outlook: Policy Scenarios to 2060* (OECD Publishing, Paris, 2022).
4. Rochman, C. M. et al. Classify plastic waste as hazardous. *Nature* **494**, 169–171 (2013).
5. Chen, L. *et al.* Micro/nanoplastics pollution poses a potential threat to soil health. *Global Change Biol.* **30**, e17470 (2024).
6. Zhang, Z. *et al.* Ecological risk assessment of marine plastic pollution. *Nat. Sustainability.* **8**, 1143–1153 (2025).
7. Chen, F., Chen, Y., Pan, K. & Liu, H. Species-specific deformation of microalgae in the presence of microplastics. *Environ. Chem. Lett.* **22**, 953–959 (2024).
8. Omura, T. *et al.* Microbial decomposition of biodegradable plastics on the deep-sea floor. *Nat. commun.* **15**, 568 (2024).
9. Yang, X., Zhang, Y., Sun, P. & Peng, C. A review on renewable energy: Conversion and utilization of biomass. *Smart Mol.* **2**, e20240019 (2024).
10. Yang, A. *et al.*, Scalable production of robust and creep resistant ultra-high filled wood-plastic composites. *Compos. Part B-Eng.* **289**, 111937 (2025).
11. González, D., Santos, V. & Parajó, J. C., Manufacture of fibrous reinforcements for biocomposites and hemicellulosic oligomers from bamboo. *Chem. Eng. J.* **167**, 278–287 (2011).
12. Hassan, S. B., Oghenevweta, J. E. & Aigbodion, V. S., Morphological and mechanical properties of carbonized waste maize stalk as reinforcement for eco-composites. *Compos. Part B-Eng.* **43**, 2230–2236 (2012).
13. Kamau-Devers, K. & Miller, S. A. The environmental attributes of wood fiber composites with bio-based or petroleum-based plastics. *Inter. J. of Life Cycle Assess.* **25**, 1145–1159 (2020).

14. Liang, G. *et al.* Structural design, performance regulation, and engineering applications of bamboo-derived micro-nano cross-linked composites. *Compos. Sci. Technol.* **281**, 111642 (2026).
15. Fang, X., Xie, Y., Li, R. & Xu, W. Ferroconcrete-inspired synergistic modification of bamboo fiber/PLA biocomposites with enhanced interfacial compatibility and antibacterial performance. *Polymer* **356**, 130089 (2026).
16. Xia, L. *et al.* Enhanced mechanical performance of bamboo fiber/polypropylene composites via micro-nano reinforcing strategy. *Compos. Part B-Eng.* **280**, 111488 (2024).
17. De, B., Bera, M., Bhattacharjee, D., Ray, B. C. & Mukherjee, S. A comprehensive review on fiber-reinforced polymer composites: Raw materials to applications, recycling, and waste management. *Prog. Mater. Sci.* **146**, 101326 (2024).
18. Hou, S.-X. *et al.* Closed-loop recyclable wood-plastic composite as a sustainable alternative to wood: A solution for utilizing wood waste and promoting carbon sequestration. *Chem. Eng. J.* **499**, 156478 (2024).
19. Hao, X. *et al.* Effects of fiber geometry and orientation distribution on the anisotropy of mechanical properties, creep behavior, and thermal expansion of natural fiber/HDPE composites. *Compos. Part B-Eng.* **185**, 107778 (2020).
20. Chen, L. *et al.* Enhancing wood-plastic composites for high-performance structural applications. *Compos. Part B-Eng.* **299**, 112410 (2025).
21. Wang, M., Jiang, G., Zeng, S., Zhao, D. & Yu, H. Reinventing Cellulose into Sustainable and Versatile Bioplastics via Molecular-Scale Design. *Research* **9**, 1289 (2026).
22. Li, Z. et al. Smart molecular design for functional cellulose gels and flexible devices. *Smart Mol.* **4**, e70038 (2026).
23. Zeng, S. *et al.* A gradient-structured all-cellulose biofoam enabled by solvent-induced molecular assembly for sustainable insulation modules. *Nat. commun.* **17**, 1913 (2026).
24. Zhang, L. et al. Bioderived Cellulose Aerogel Fibers with Hierarchical Porosity for Millisecond Hydrovoltaic Sensing. *Research* **9**, 1324 (2026).
25. Zhang, K. et al. Mechanical/thermomechanical–electromagnetic multifunctional cellulose nanofibril-MXene aerogel-based metamaterials. *Research* **8**, 0900 (2025).
26. Li, X. et al. Balancing mechanical-thermal-electrical properties in cellulose ionogels via crystallization-induced molecular assembly. *Nat. commun.* **16**, 9970 (2025).
27. Long, Q. et al. A cellulose ionogel with rubber-like stretchability for low-grade heat harvesting. *Research* **7**, 0533 (2024).
28. Chen, L. et al. Cellulose nanocomposites by supramolecular chemistry engineering. *Nat. Rev. Mater.* **10**, 728–749 (2025).
29. Chen, S. et al. Kinetic Molecular Modulation of Highly-Aligned Self-Locking Nanofibers for Strong, Tough, and Transparent Bioplastic Films. *Adv. Funct. Mater.* **36**, e20770 (2026).

30. Huang, Z. et al. Hydro-Responsive Topological Engineering of Cellulose Bioplastics via Dynamic Imine Bonds for Water-Assisted Reprocessing and Closed-Loop Sustainability. *ACS Sustainable Chem. Eng.* **14**, 4181–4192 (2026).
31. Tang, H. et al. High-strength, multi-mode processable bamboo molecular bioplastic enabled by solvent-shaping regulation. *Nat. commun.* **16**, 8729 (2025).
32. Li, J. *et al.* Stimulus-Induced Self-Reinforcement in Supramolecular Bamboo Plastics toward Mechanical Robustness and Programmable Shapeability. *Adv. Sci.* **13**, e74426 (2026).
33. Zeng, S. *et al.* Cellulosic Engineering Plastic with High Shapeability, Recyclability, Lightweight and High-Strength Properties. *Adv. Mater.* **38**, e73129 (2026).
34. Zhao, D. et al. A stiffness-switchable, biomimetic smart material enabled by supramolecular reconfiguration. *Adv. Mater.* **32**, 2107857 (2022).
35. Zhou, J. *et al.* Biodegradable, Thermally Stable, and Programmable Cellulosic Bioplastics Enabled by Supramolecular Stimulated Mediation. *Research* **9**, 1098 (2026).
36. Lin, C. et al. Supramolecular polymers with water-triggered dense domains enabling mechanical robustness programmability and weather resistance. *Nat. commun.* (2026).
37. Qiu, Y. *et al.* Coassembly of hybrid microscale biomatter for robust, water-processable, and sustainable bioplastics. *Sci. Adv.* **11**, eadr1596 (2025).
38. Xie, D. *et al.* Nacre-inspired starch-based bioplastic with excellent mechanical strength and electromagnetic interference shielding. *Carbohydr. Polym.* **331**, 121888 (2024).
39. Liu, Y. et al. Stretchable, self-healing, and processable bioelastomers enabled by highly branched cross-linking networks for flexible electronics. *Research* **9**, 1391 (2026).
40. Wang, C. *et al.* Sustainable and versatile bioplastics toward large-scale industrialization. *Chem. Eng. J.* **521**, 167070 (2025).
41. Xia, Q. *et al.* Photosynthesis-Inspired Enhancement of Cellulose Bioplastics Using Hemicellulose-Derived Biodegradable Polyesters. *Adv. Funct. Mater.* **35**, 2417076 (2025).

Figures

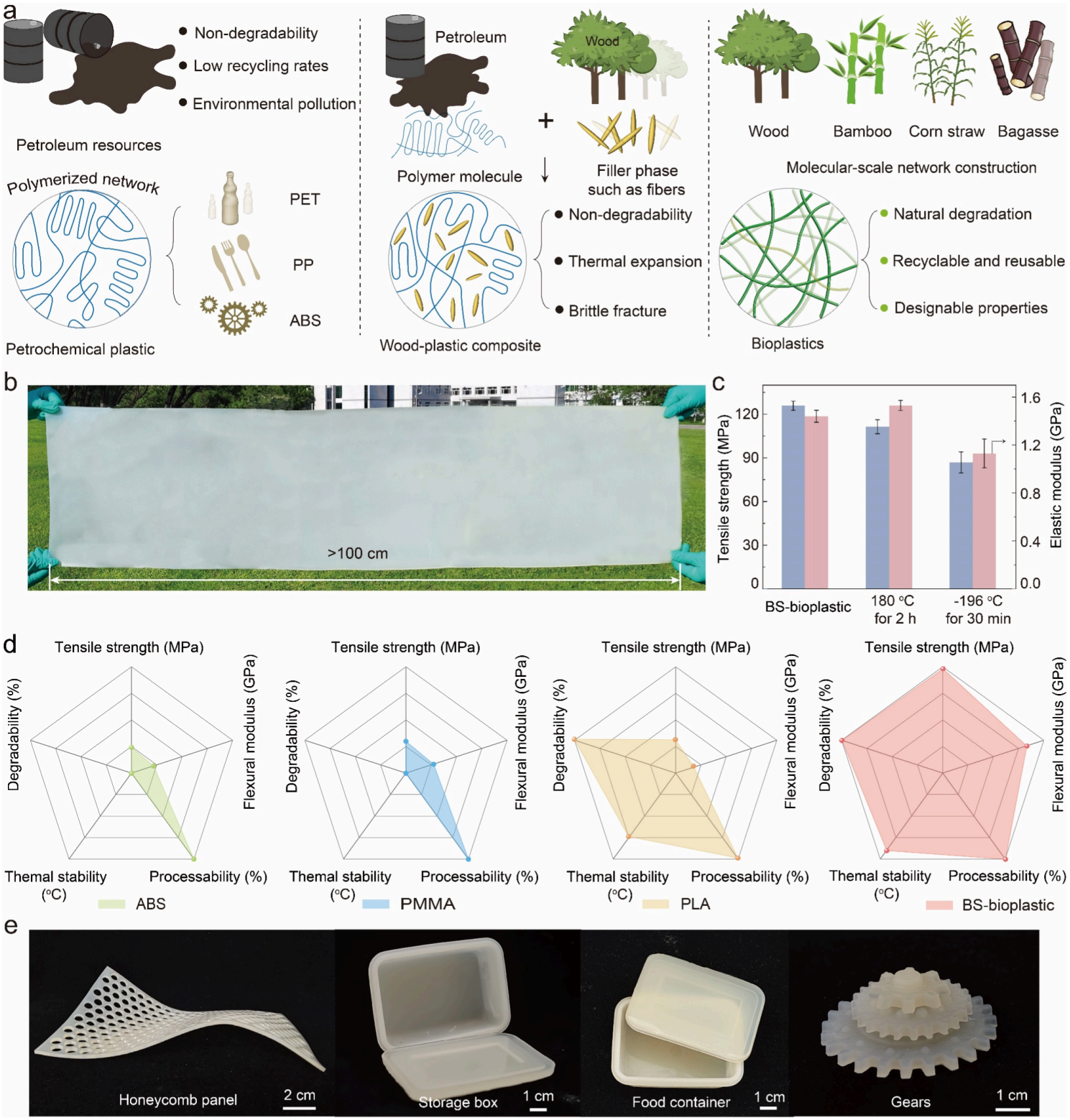


Figure 1

Development and fabrication of BS–bioplastic. a Comparison of petrochemical plastics, wood–plastic composites, and bioplastics. **b** Demonstration of the large-scale preparation of BS–bioplastic. **c** Comparison of tensile strength and elastic modulus of BS–bioplastic after exposure to −196 °C for 30 min and 180 °C for 2 h, respectively. **d** Radar plot to compare BS–bioplastic and some commercial plastics. **e** Processability and formability of BS–bioplastic for various bioplastic products.

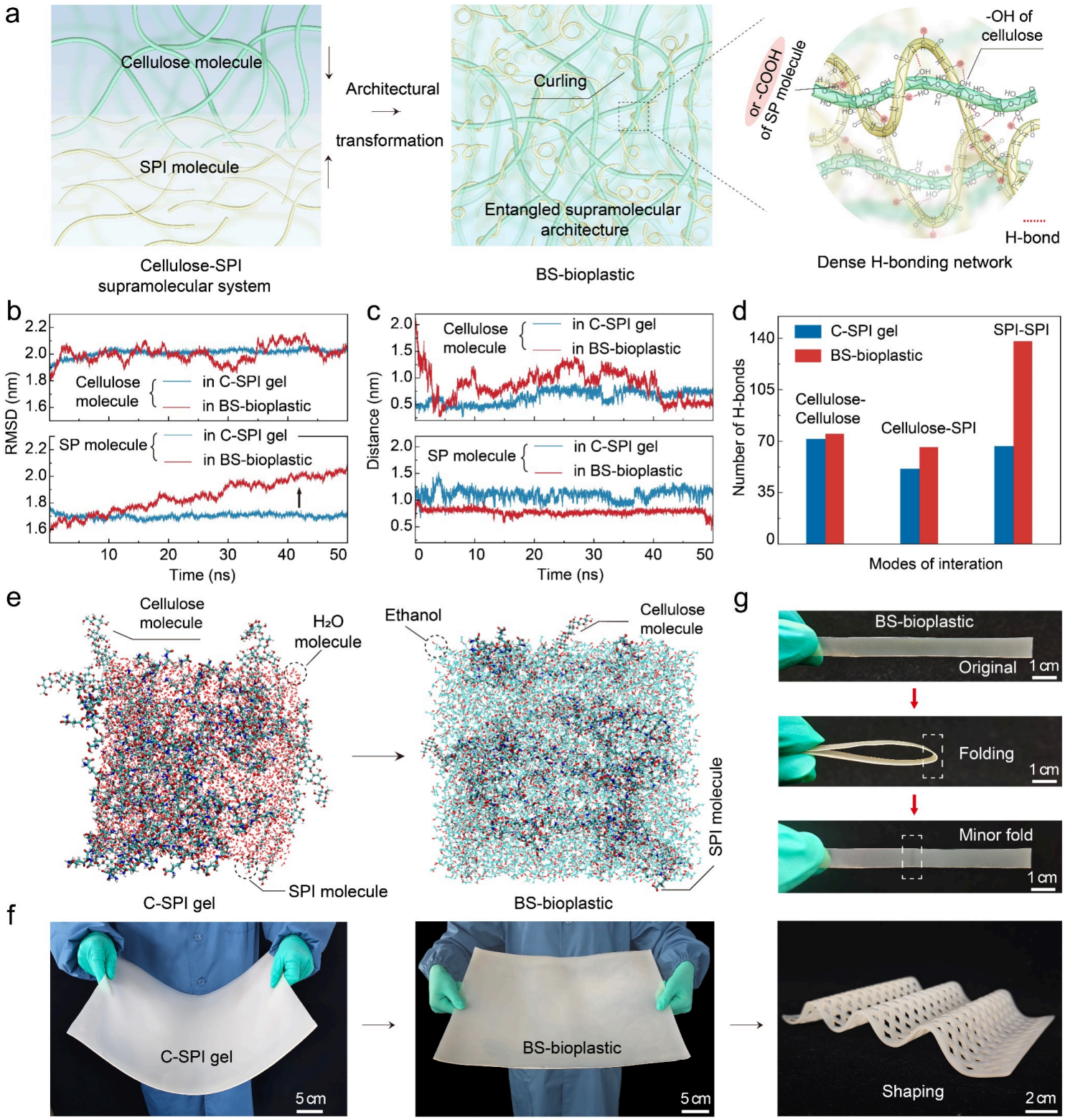


Figure 2

MD simulation analysis of BS–bioplastic. a Mechanism diagram of BS–bioplastic. Each element of schematic diagram was conceived by the authors of this work. **b**Investigating the RMSD values of cellulose molecules and SPI moleculesduring different conditions. **c**End-to-end distance of cellulose and SPI molecules during different systems. **d** Number of H-bonds between C–SPI gel and BS–bioplastic. **e**MD snapshots of C–SPI gel and BS–bioplastic. **f** Optical images of the changes from C–SPI gel to BS–

bioplastic during the final processing and molding. **g**Optical images of BS–bioplastic demonstrate robust foldability.

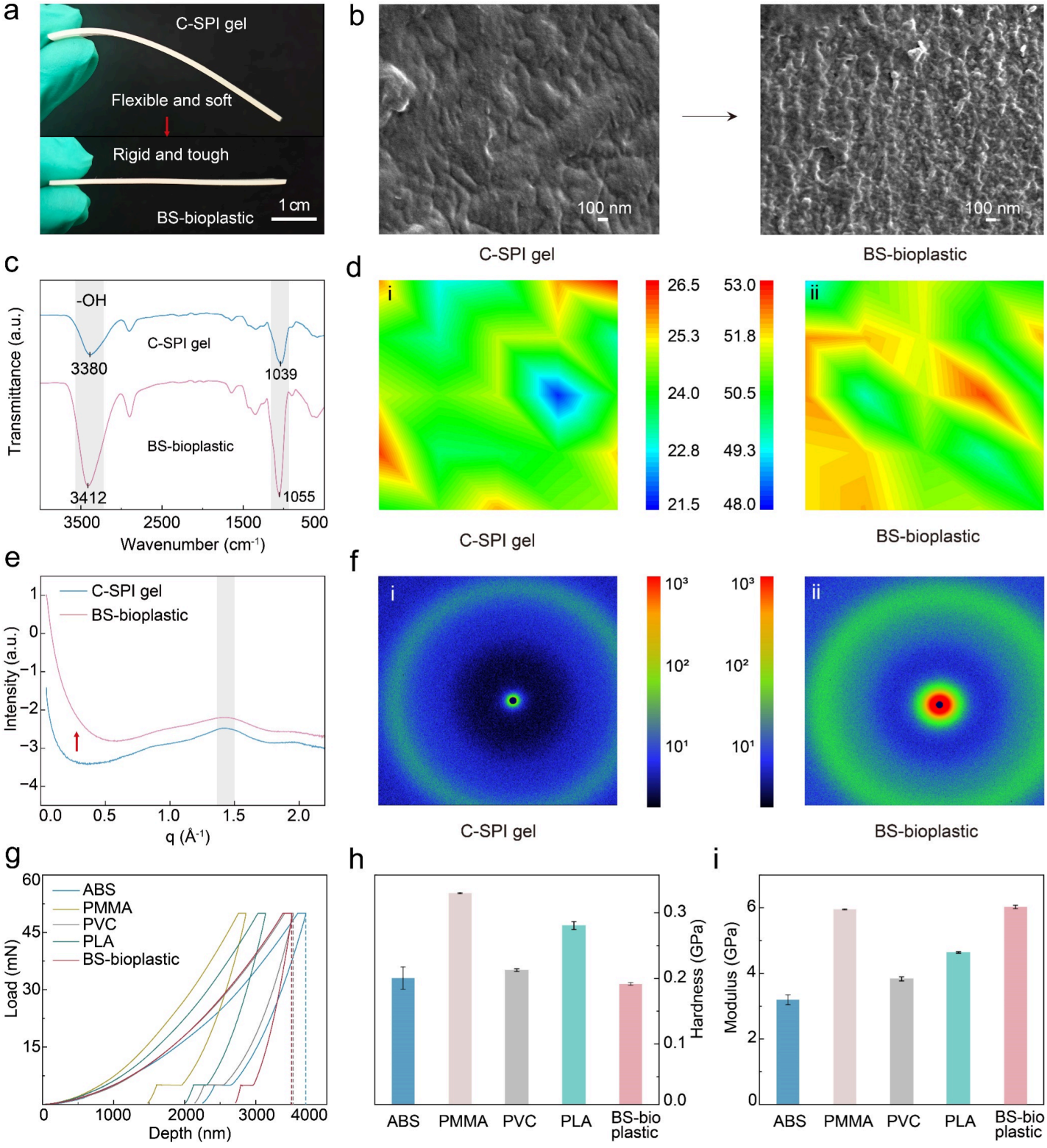


Figure 3

Structures and characterizations of BS–bioplastic. a Optical images of flexible and soft C–SPI gel and rigid and tough BS–bioplastic. **b** SEM images of C–SPI gel and BS–bioplastic. **c-d** FTIR spectrum and 2D

FTIR of C–SPI gel and BS–bioplastic. **e-f** Nanoscale characterization of C–SPI gel and BS–bioplastic represented by WAXS pattern and 2D WAXS images. **g-i** Comparison of the load–depth curves, hardness, and modulus of BS–bioplastic and commercial plastics via static nanoindentation tests.

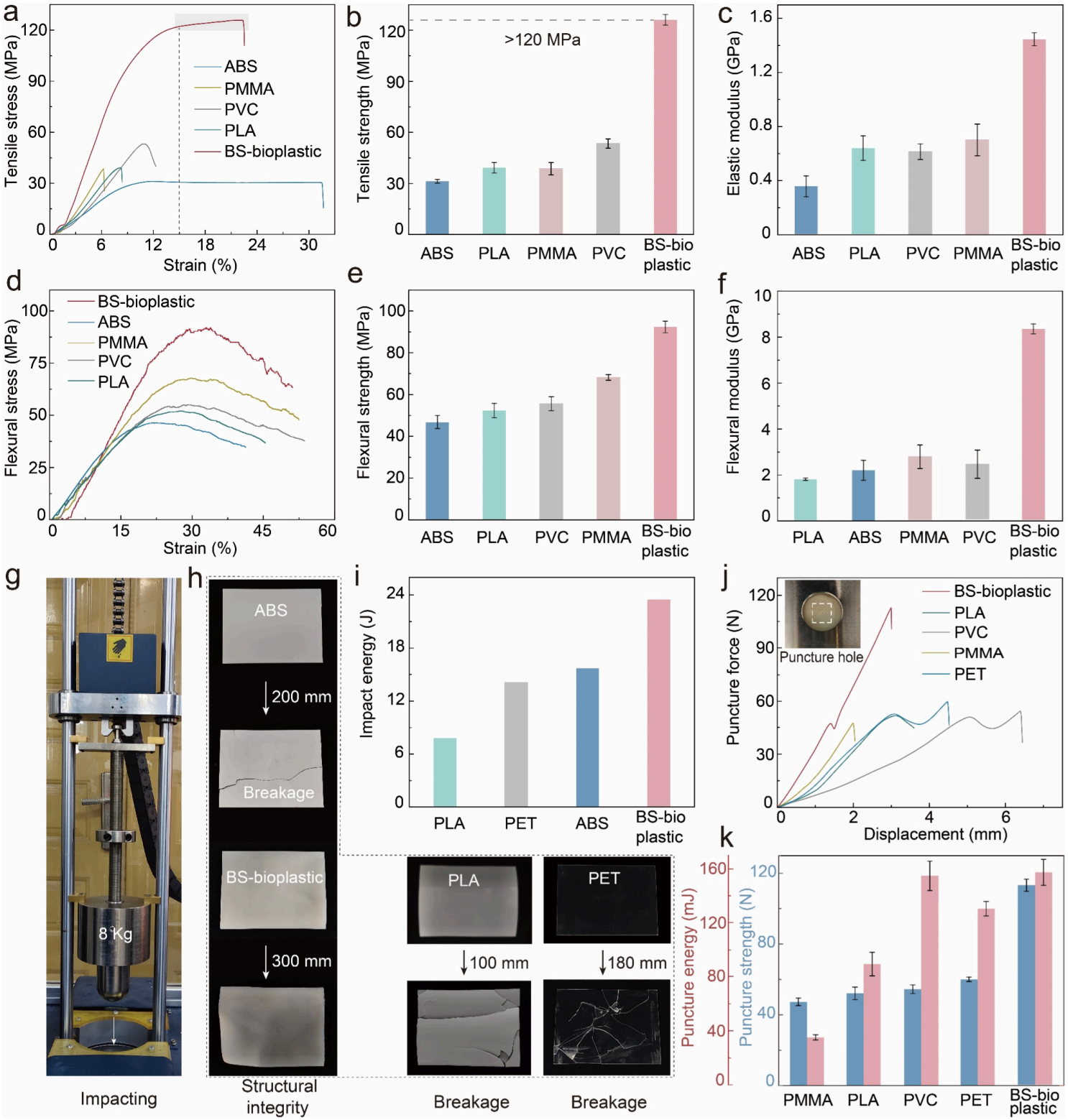


Figure 4

Mechanical properties of BS–bioplastic. a-c Comparison of tensile stress-strain curves (**a**), tensile strength (**b**), and elastic modulus (**c**) of BS–bioplastic and several commercial plastics (ABS, PLA, PMMA, PVC). **d-f** Comparison of flexural stress-strain curves (**d**), bar charts of flexural strength (**e**), and flexural modulus (**f**) for BS–bioplastic and commercial plastics. **g** Digital photos of the drop hammer impact test for BS–bioplastic and commercial plastics. **h** Optical images of the plastics before and after impacting process. **i**Comparison of the impact energy of BS–bioplastic and commercial plastics. **j**Puncture force-displacement curves. The inserted image shows an actual BS–bioplastic specimen after puncture. **k** Comparison of the puncture strength and puncture energy of BS–bioplastic and commercial plastics.

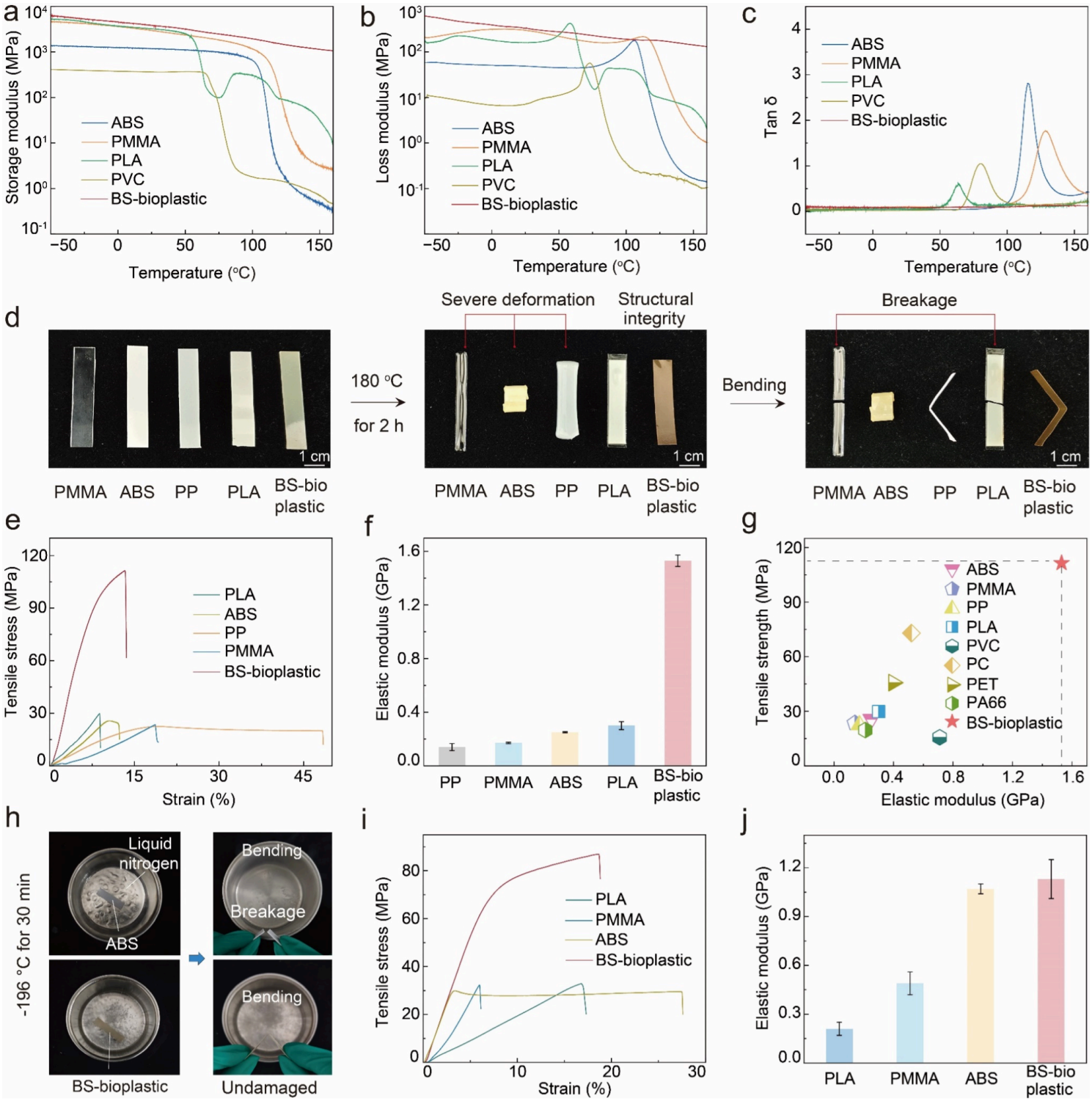


Figure 5

Structural stability and mechanical performance of BS–bioplastic at low and high temperatures. a-c DMA curves of BS–bioplastic and various commercial plastics of the storage modulus (**a**), loss modulus (**b**), and tan δ (**c**). **d** Optical images of BS–bioplastic, ABS, PMMA, PP, and PLA exposed to 180 °C for 2 h. **e-f** Comparison of tensile stress-strain curves (**e**), and elastic modulus (**f**) of BS–bioplastic and commercial plastics after being exposed to 180 °C for 2 h. **g** Investigating the tensile strength and modulus between BS–bioplastic and commercial plastics after being exposed to 180 °C for 2 h. **h**

Optical images of BS–bioplastic and ABS were exposed to liquid nitrogen (−196 °C) for 30 min. **i-j**Comparison of tensile stress-strain curves (**i**), and elastic modulus (**j**) of BS–bioplastic and commercial plastics.

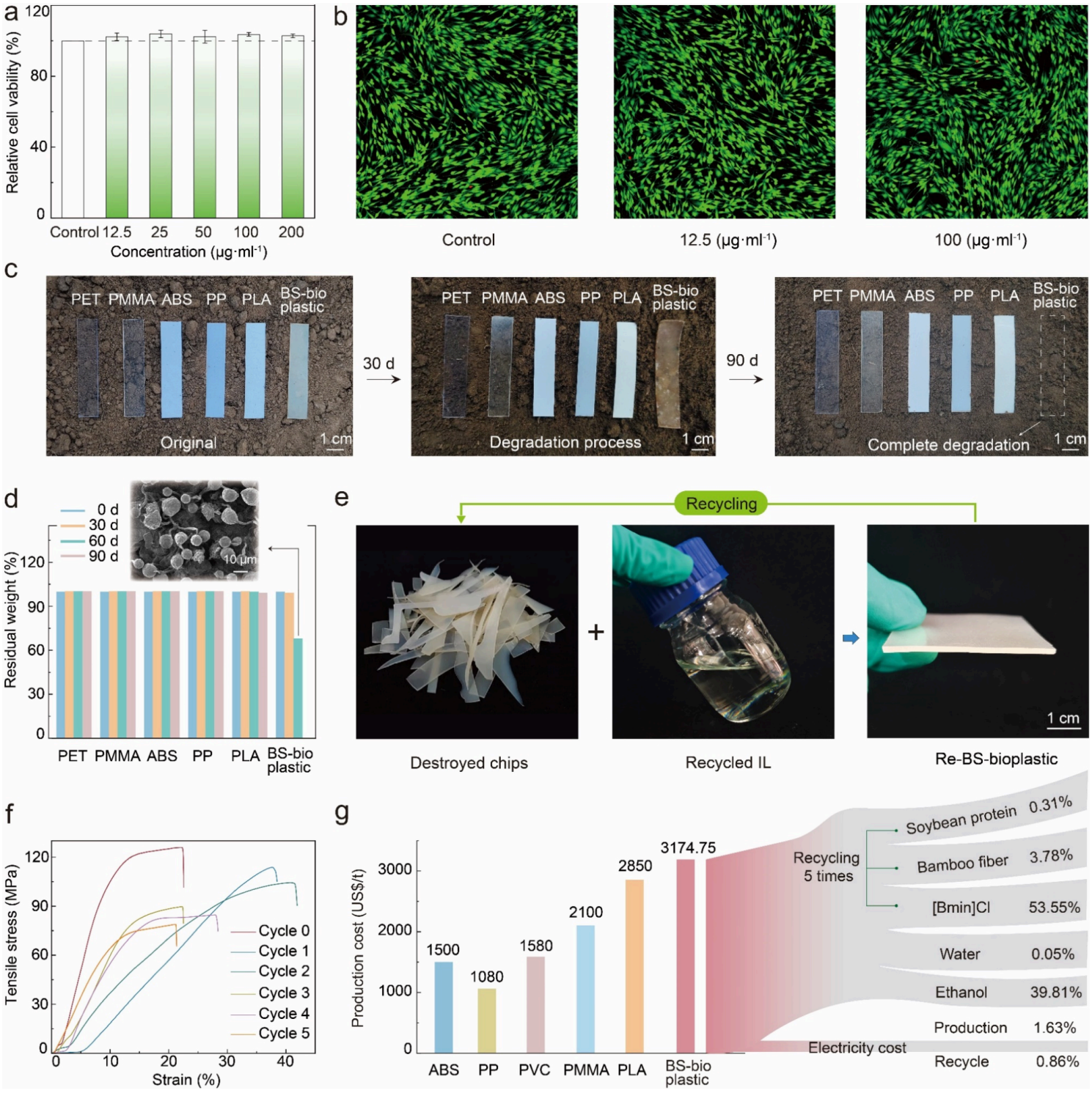


Figure 6

The biodegradability, recyclability, and economic feasibility of BS–bioplastic. a Investigating the cell viability of BS–bioplastic in different cell suspension concentrations. **b** Live staining confocal images of human fibroblasts co-cultured with different concentrations of BS–bioplastic for 24 h. **c** The

biodegradability tests of BS–bioplastic and various commercial plastics under natural soil. **d**Comparison of the residual weight ratio of BS–bioplastic and several commercial plastics. Inset shows the SEM image of BS–bioplastic degradation after 60 days. **e** Investigating the recyclability of BS–bioplastic. **f** The tensile stress-strain curves of recycled BS–bioplastic. **g** Comparison production cost of BS–bioplastic and commercial plastics.

Supplementary Files

This is a list of supplementary files associated with this preprint. Click to download.

- SupplementaryInformation.docx